Acta Cryst. (1997). D**53**, 290–301

X-ray Structure of a Ribonuclease A–Uridine Vanadate Complex at 1.3 Å Resolution

JANE E. LADNER,[a] BRIAN D. WLADKOWSKI,[a,b] L. ANDERS SVENSSON,[a,c] LENNART SJÖLIN[d] AND GARY L. GILLILAND[a]*

[a]*The Center for Advanced Research in Biotechnology of the University of Maryland Biotechnology Institute and National Institute of Standards and Technology, 9600 Gudelsky Dr., Rockville, MD 20850, USA,* [b]*Department of Chemistry, Western Maryland College, Two College Hill, Westminster, MD 21157, USA,* [c]*Department of Molecular Biophysics, Center for Chemistry and Chemical Engineering, Lund University, Box 124, S-221 00 Lund, Sweden, and* [d]*Department of Inorganic Chemistry, Chalmers University of Technology and The University of Goteborg, S-412 96 Goteborg, Sweden. E-mail: gary@ibm3.carb.nist.gov*

(*Received 12 February 1996; accepted 23 December 1996*)

Abstract

The X-ray crystal structure of a uridine vanadate–ribonuclease A complex has been determined at 1.3 Å resolution. The resulting structure includes all 124 amino-acid residues, a uridine vanadate, 131 water molecules, and a single bound 2-methyl-2-propanol. Side chains of 11 surface residues showing discrete disorder were modeled with multiple conformations. The final crystallographic *R* factor is 0.197. Structures obtained from high-level *ab initio* quantum calculations of model anionic oxyvanadate compounds were used to probe the effects of starting structure on the refinement process and final structure of the penta-coordinate phosphorane analog, uridine vanadate. The least-squares refinement procedure gave rise to the same final structure of the inhibitor despite significantly different starting models. Comparison with the previously determined complex of ribonuclease A with uridine vanadate obtained from a joint X-ray/neutron analysis (6RSA) [Wlodawer, Miller & Sjölin (1983). *Proc. Natl Acad. Sci. USA*, **80**, 3628–3631] reveals similarities in the overall enzyme structure and the relative position of the key active-site residues, His12, His119 and Lys41, but significant differences in the V—O bond distances and angles. The influence of ligand binding on the enzyme structure is assessed by a comparison of the current X-ray structure with the phosphate-free ribonuclease A structure (7RSA) [Wlodawer, Svensson, Sjölin & Gilliland (1988). *Biochemistry*, **27**, 2705–2717]. Ligand binding alters the solvent structure, distribution and number of residues with multiple conformations, and temperature factors of the protein atoms. In fact, the temperature factors of atoms of several residues that interact with the ligand are reduced, but those of the atoms of several residues remote from the active site exhibit marked increases.

1. Abbreviations

RNase A, bovine ribonuclease A; TBP, trigonal bipyramid; UV, uridine vanadate; UV–RNase, uridine vanadate–ribonuclease A complex; EOV^-, monoanionic pentacoordinate cyclic ethylene oxyvanadate; EOV^{2-}, dianionic pentacoordinate cyclic ethylene oxyvanadate; TZP, a full triple-ζ basis set for all atoms with contractions of (10*s*,6*p*)/[5*s*,3*p*] for C and O, (5*s*)/[3*s*] for H and (14*s*,11*p*,6*d*)/[10*s*,8*p*,3*d*] for V (Wachters, 1970) with a single polarization function appended to C, O and V; RHF, restricted Hartree–Fock method (Hehre, Radom, Schleyer & Pople, 1986); MP2, second-order Møller–Plesset perturbation theory; *B* factor, temperature-factor value.

2. Introduction

Bovine pancreatic ribonuclease A (E.C. 3.1.27.5; RNase A), a protein composed of a single chain of 124 amino-acid residues, efficiently catalyzes the hydrolysis of phosphate–ester linkages in single-stranded RNA. Since the determination of the crystal structure nearly 30 years ago (Avey *et al.*, 1967; Kartha, Bello & Harker, 1967), RNase A and its subtilisin-cleaved form, RNase S, (Richards & Vithayathil, 1959) have continued to be the subject of crystallographic studies using both X-ray and neutron diffraction techniques (*e.g.* Wyckoff *et al.*, 1970; Wlodawer, Bott & Sjölin, 1982; Wlodawer & Sjölin, 1983; Borkakoti, Moss, Stanford & Palmer, 1984; Campbell & Petsko, 1987; Wlodawer, Svensson, Sjölin & Gilliland, 1988; Svensson, Sjölin, Dill & Gilliland, 1991; Kim, Varadarajan, Wyckoff & Richards, 1992). These studies have extended the structure determination to high resolution providing details of the atomic structure. The structures determined include the enzyme with a phosphate or sulfate ion bound in the active site and the unligated form. The crystal structures of complexes of RNase with various inhibitors and nucleotide analogs have also been determined, leading to a further understanding of the structural features essential for substrate binding and enzyme catalysis (*e.g.*, Richards & Wyckoff, 1971; Wodak, Liu & Wyckoff, 1977; Howlin, Harris, Moss & Palmer, 1987; Zegers *et al.*, 1994). In addition, structural

investigations of semisynthetic variants of RNase have been carried out to probe the catalytic mechanism (*e.g.*, Taylor, Kormoriya & Chaiken, 1985; Martin, Doscher & Edwards, 1987; Varadarajan & Richards, 1992).

The generally accepted mechanism by which RNase A catalyzes phosphate–ester hydrolysis is a two-step general-acid/general-base mechanism. In the first step, the 3′-5′ phosphate linkage is cleaved *via* intramolecular transphosphorylation leading to a 2′-3′ cyclic phosphate intermediate. Subsequently, the cyclic phosphate is hydrolyzed by a water molecule to form a 3′ monophosphate–ester as the final product. Both steps in the reaction are known to proceed by an in-line inversion displacement mechanism based on isotopic labeling experiments (Usher, Richardson & Eckstein, 1970; Usher, Erenrich & Eckstein, 1972). Consistent with these features, a penta-coordinate trigonal bipyramid (TBP) phosphorane is postulated to be an important structure along the reaction pathway.

Lindquist, Lynn & Lienhard (1973) proposed that a complex of uridine with oxy-vanadium compounds, that can achieve a penta-coordinate arrangement, might be stable analogs for the TBP phosphorane structure believed to be an intermediate in the mechanism. Consistent with expectations, several vanadate species were found to be potent inhibitors for related enzymes including ATPases, phosphatases and nucleases (see Crans, Willging & Butler, 1990, and references therein). In contrast to the extensive solution-phase studies by Crans and others, only a few vanadate–enzyme complexes have been studied crystallographically: uridine vanadate (UV) bound to bovine RNase A (UV–RNase A) (Alber, Gilbert, Ponzi & Petsko, 1983; Wlodawer, Miller & Sjölin, 1983; Borah *et al.*, 1985); *Aspergillus orzae* RNase T_1-H_2VO_4- (Kostrewa, Choe, Heinemann & Saenger, 1989); and rat acid phosphatase (Lindqvist, Schneider & Vihko, 1994). Surprisingly, a penta-coordinate oxyvanadate has been observed crystallographically in only two of these three systems, bovine RNase A and rat acid phosphatase.

Structural reports of two different crystal-structure complexes of RNase A with the UV inhibitor have been reported (Alber *et al.*, 1983; Wlodawer & Sjölin, 1983), and one of these has been compared with the results of high-field NMR studies (Borah *et al.*, 1985). The first of these analyses reported that the presence of the transition-state like analog reduced the mobility of the side chain of Lys41 because of its direct interaction with the ligand (Alber *et al.*, 1983). The second structure of UV–RNase A, determined using combined 2.0 Å X-ray and 2.2 Å neutron data (Wlodawer & Sjölin, 1983), and its comparison with the NMR results (Borah *et al.*, 1985) revealed that similar to the earlier results, Lys41, His12, and His119 side chains were in direct contact with UV. However, the interactions were inconsistent with expectations based on the proposed mechanism. His12 interacts with an equatorial vanadate O atom and Lys41 was found closest to the axial O2′ atom. Recently, UV–RNase A has been investigated using one- and two-dimensional NMR techniques (Veenstra & Lee, 1994). Based on the appearance or absence of certain cross-peaks in the NMR spectrum, the position of the of His119 was postulated to be different for the complex in solution than in the crystal structure.

Although an array of critical information about how RNase A functions to catalyze the hydrolysis of phosphate–ester linkages has been determined from the structural studies, the actual character of the TBP vanadate structure including its protonation state and whether it represents a transition state or a true intermediate continues to be an issue of considerable debate. In the study presented here, the UV–RNase A structure has been extended to 1.3 Å resolution. The refinement process and the interpretation of the final structure are aided by high-level *ab initio* quantum mechanical results on model oxyvanadates. The analysis of the three-dimensional structure and the first comparison with unligated RNase A (Wlodawer *et al.*, 1988) provide a detailed picture of the changes induced in the enzyme structure upon ligand binding.

3. Materials and methods

3.1. *Crystallization and inhibitor complex formation*

RNase A crystals used in the X-ray diffraction experiments were grown by previously described procedures (Wlodawer *et al.*, 1982, 1983). Briefly, single crystals of RNase A were obtained at room temperature from solutions containing 100 mg ml^{-1} RNase A and 43% 2-methyl-2-propanol at pH 5.3. The UV solution was prepared by mixing 45 mg of uridine and 105 mg of NH_4VO_3 in 6.1 ml of 50 m*M* imidazole buffer followed by heating to 333 K for 30 min using a hot plate. The resulting solution was yellow, and exhibited a pH of 5.2. New synthetic mother liquor was prepared by the addition of 2-methyl-2-propanol to the UV solution to obtain a solution that contained 50%(*v*/*v*) alcohol. The final pH of the solution was 6.2. Crystals were transferred to 1 ml of synthetic mother liquor (without protein) and allowed to soak. All crystals became dark green during the soaking period. For data collection, a crystal soaked for 10 d was used.

3.2. *X-ray data collection and processing*

Diffraction data were collected using a Siemens electronic area detector mounted on a Siemens* three-axis camera controlled by a PCS Cadmus 9900 microcomputer. X-rays were generated with a Rigaku RU-200

* Certain commercial equipment, instruments, and materials are identified in this paper to specify the experimental procedure. Such identification does not imply recommendation or endorsement by the National Institute of Standards and Technology, nor does it imply that the material or equipment identified are necessarily the best available for the purpose.

Table 1. *Details of relevant structure determinations of RNase A*

	1RUV	6RSA*	7RSA†
Active site	Uridine vanadate	Uridine vanadate	—
Space group	$P2_1$	$P2_1$	$P2_1$
Unit-cell parameters			
a (Å)	29.80	30.30	30.20
b (Å)	38.20	38.40	38.40
c (Å)	53.20	53.70	53.30
β (°)	106.10	106.40	105.90
Diffraction data radiation	X-ray	X-ray/ Neutron	X-ray
Resolution (Å)	1.25	2.00	1.26
No. observed reflections	94196	15451	129732
No. unique reflections	25327	6617	25732
No. possible reflections	30307	8188	30749
R_{sym}	0.05	0.07	0.05
Refinement procedure	*PROFFT*‡	*PROLSQ*§	*PROFFT*‡
Resolution limits (Å)	10.0–1.25	10.0–2.0	10.0–1.26
R factor	0.197	0.188 (X-ray) 0.199 (neutron)	0.150
R.m.s. deviations			
Bond length (Å)	0.027	0.023	0.024
Angle distance (Å)	0.038	—	0.038
Planarity (Å)	0.017	—	0.017
Ideal chirality (Å)	0.168	—	0.188

*Wlodawer, Miller & Sjolin (1983). †Wlodawer, Svensson, Sjölin & Gilliland (1988). ‡Finzel (1987). §Wlodawer & Hendrickson (1982).

HB rotating anode operating at 40 kV and 100 mA with a 0.3 × 3.0 mm focal spot. A graphite monochromator was used to select the Cu $K\alpha$ wavelength, and a 0.5 mm collimator was used. During the data collection, the area-detector chamber was mounted 10 cm from the crystal, and the carriage angles were set at 26 and 47°, thus, intercepting data from infinity to 1.25 Å resolution. Each electronic image of the diffraction data collected represents a 0.25° oscillation counted for 5 min at the largest carriage angle. All data collection was carried out at 293 ± 2 K. The determination of unit-cell parameters, crystal orientation and the integration of reflection intensities were performed with the *XENGEN* program system (Howard *et al.*, 1987). Summaries of the X-ray data collection and processing statistics are given in Table 1.

3.3. *Structure determination and restrained least-squares refinement*

The X-ray structure of UV–RNase A was solved by analysis of difference Fourier maps followed by least-squares refinement. The initial map was calculated using the coordinates from the 1.26 Å phosphate-free structure of RNase A (Wlodawer *et al.*, 1988). The least-squares refinement of the X-ray structure was accomplished using the programs *PROLSQ* (Hendrickson & Konnert, 1980) and *PROFFT* (Finzel, 1987; Sheriff, 1987).

Initially, a UV standard group was constructed using *SYBYL*™ and information from theoretical calculations (Krauss & Basch, 1992). Only adjustments of torsion angles were required to fit the inhibitor into the difference Fourier map. The phases of this map were calculated using only the protein heavy atoms. During the refinement no restraints were placed on the bond angles of the vanadate O atoms, whereas standard restraints were placed on the remaining part of the inhibitor and on the enzyme. After an initial adjustment of the model and inclusion of H atoms, typically 15 cycles of least-squares refinement were performed before the model was re-examined and adjusted using the computer graphics programs *FRODO* (Jones, 1978) and *O* (Jones, Zou, Cowan & Kjeldgaard, 1991). A series of six refinement and rebuilding cycles was needed to minimize significant peaks in the $F_o - F_c$ difference Fourier maps.

Following the initial stages of refinement, the structural data from the model oxyvanadate compounds determined computationally were used to address whether UV is likely to be mono- or dianionic within the RNase active site, and to examine the effect of the UV standard group on the refinement process. The mono- and dianionic UV models used in this study as starting points in the X-ray refinement process are the penta-coordinate cyclic ethylene oxyvanadates compounds (EOV^- and EOV^{2-}), shown in Figs. 1(*a*) and 1(*b*), respectively. The atomic orbital basis set used to generate these structures include a full triple-ζ basis on all atoms with contractions of (10*s*,6*p*)/[5*s*,3*p*] for C and O, (5*s*)/[3*s*] for H, and (14*s*,11*p*,6*d*)/[10*s*,8*p*,3*d*] for V (Wachters, 1970) with a single polarization function appended to C, O and V (TZP). The electronic wavefunctions were determined by the single-reference, self-consistent-field, restricted Hartree–Fock (RHF) method (Hehre *et al.*, 1986), and dynamical electron correlation effects were estimated for using second-order Møller–Plesset (MP2) perturbation theory (Hehre *et al.*, 1986). The core orbitals were excluded from the active space in all correlated calculations. RHF and MP2 analytic gradient techniques were used to determine the optimized structures to 10^{-3} Å or rad in the internal coordinate space. All calculations were performed using the *GAUSSIAN*92 (Frisch *et al.*, 1992) program package.

Two independent refinements were initiated using either a mono- or a dianionic standard group based on structures calculated at the TZP RHF level of theory. The refinements were carried out in parallel using identical protocols. After 30 cycles of refinement, the resulting UV structures retained significant differences, particularly in the V—O bond distances. Before continuing, the refined UV coordinates of each structure were used to produce a new standard group for the restraints dictionary. An additional six cycles of refinement were performed using the updated restraints. After three iterations, the refinements converged to the same structure. Two additional independent refinements

were carried out using the mono- and dianionic starting models with all V—O bond restraints removed from the restraints dictionary. Convergence to the same structure was reached after six refinement cycles. The results were then compared with those of the iterative procedure to assess if both methods of refinement converged to the same structure.

The positions for all residues modeled with alternate conformations were verified by omit maps. Side chains of the residues with alternate conformations were removed and five cycles of refinement were carried out before recalculating the electron-density map The final coordinates have been deposited in the Brookhaven Protein Data Bank (Bernstein *et al.*, 1977).*

* Atomic coordinates and structure factors have been deposited with the Protein Data Bank, Brookhaven National Laboratory (Reference: 1RUV, R1RUVSF). Free copies may be obtained through The Managing Editor, International Union of Crystallography, 5 Abbey Square, Chester CH1 2HU, England (Reference: gr0630).

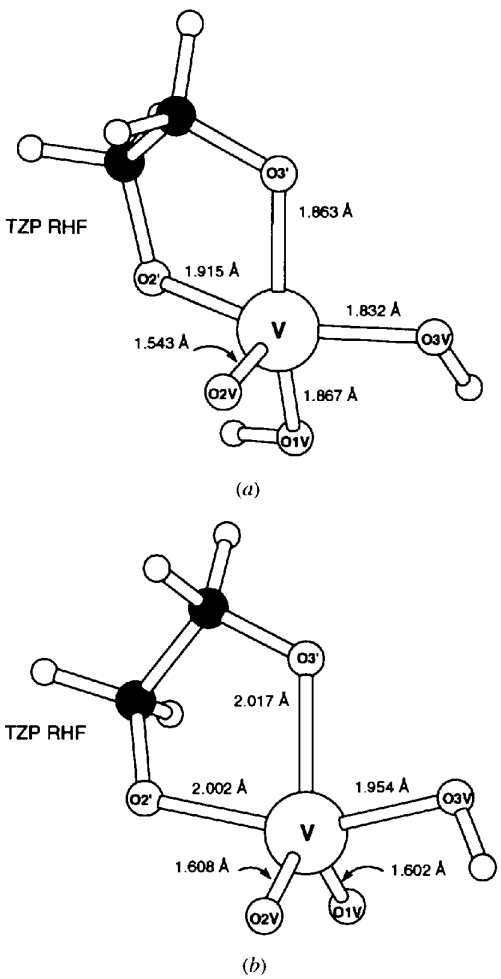

Fig. 1. The *ab initio* models calculated at the TZP RHF level of theory for (*a*) the monoanionic ethylene oxyvanadate compound (EOV^-) and (*b*) the dianionic ethylene oxyvanadate compound (EOV^{2-}).

3.4. *Structure comparisons*

The final UV–RNase A structure, 1RUV, reported here is compared with the unliganded RNase A structure, 7RSA (Wlodawer *et al.*, 1988) determined at 1.26 Å resolution, as well as with an earlier UV–RNase A structure, 6RSA, refined using both X-ray and neutron data determined at 2.0 and 2.2 Å, respectively (Wlodawer *et al.*, 1983; Borah *et al.*, 1985). Crystals used to obtain the 6RSA, 7RSA and 1RUV structures were grown using the same protocol and, therefore, represent appropriate models for comparison. Superpositioning of the molecules was performed with the *ALIGN* program (Satow, Cohen, Padlan & Davies, 1986) using only the C^α-atom positions of the polypeptide backbone. Finally, in order to probe the changes in mobility of RNase A as UV binds, temperature-factor values (*B* factors) were compared for both the main-chain and side-chain atoms of 7RSA and 1RUV. The UV–RNase A complex *B* factors were normalized to those obtained for the unligated 7RSA structure. The *B*-factor values were scaled to 7RSA by superimposing the population distributions of values of the square root of *B*. This can be done because the population of *B* factors can be approximated by a Gaussian squared function. The differences in the average *B* factors between the two structures were then determined for each residue in the protein.

4. Results

4.1. *High-resolution X-ray crystal structure of the UV–RNase A complex*

The crystallographic refinement of UV–RNase A presented here is based on interpretation of the electron-density map accounting for all 124 amino-acid residues in the protein, the UV inhibitor, 131 water molecules, and a single 2-methyl-2-propanol molecule. A total of 11 surface residues (Ser15, Ser16, Ser18, Asn24, Gln28, Ser32, Ser50, Ser59, Val63, Ser77 and Asp83) were modeled with two conformations. The final UV–RNase A structure has a crystallographic *R* factor of 0.197. Summaries of the refinement statistics for 1RUV and of two other RNase structures that are compared are given in Table 1. The quality of the current phases based on 1RUV is illustrated by the $2F_o - F_c$ electron-density map of the active-site region shown in Fig. 2. A C^α representation of the final UV–RNase A structure including the UV and the amino-acid residues with multiple conformations is shown in Fig. 3.

The UV binding site of RNase A is divided into three regions, the P_1, R_1, and B_1 subsites corresponding to the uridine base, the ribose ring, and the TBP vanadate, respectively. Each subsite is defined to include all amino-acid residues and water molecules within 4.0 Å of appropriate atoms of the UV inhibitor. The B_1 pyrimidine-binding subsite formed by His12, Val43, Asn44, Asn45, Arg83, Phe120 and three water molecules

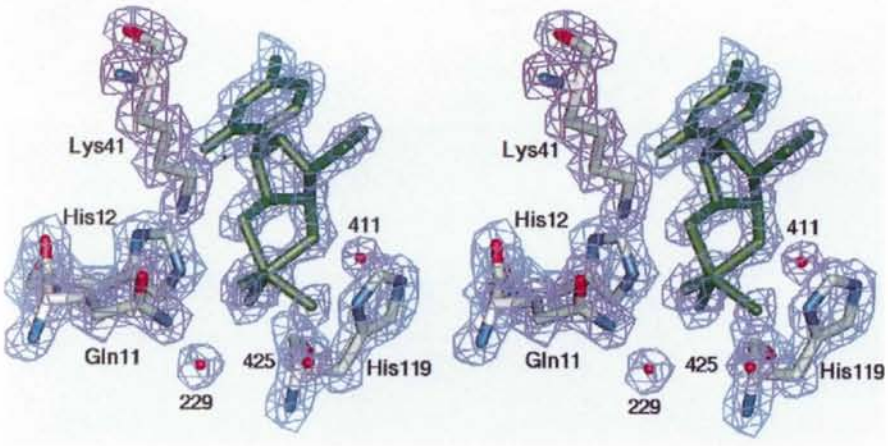

Fig. 2. A representative sample of the final $2F_o - F_c$ electron-density map of the UV–RNase A complex in the vicinity of the uridine binding site contoured at 1.0σ.

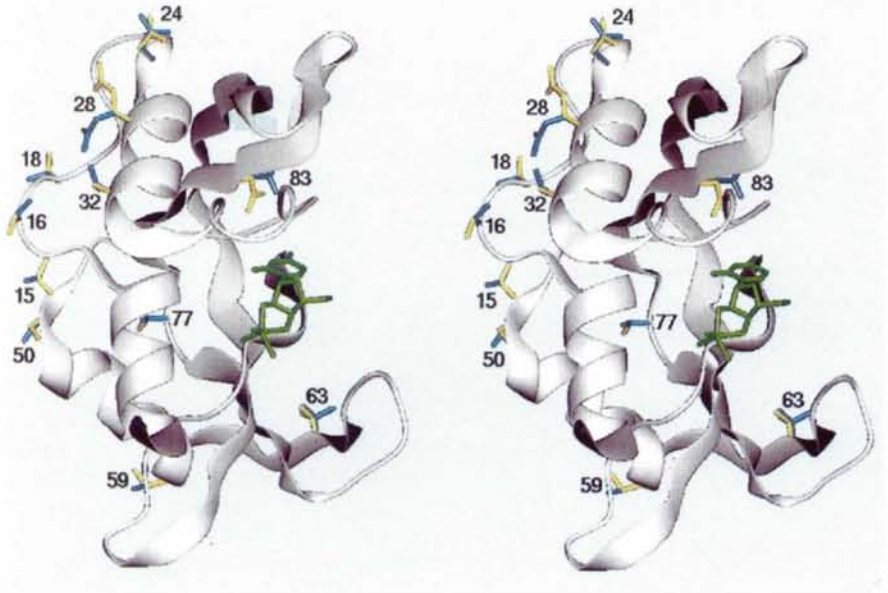

Fig. 3. The C^{α} backbone of ribonuclease A with UV bound in the active site. The side chains of the residues refined with multiple conformations are shown.

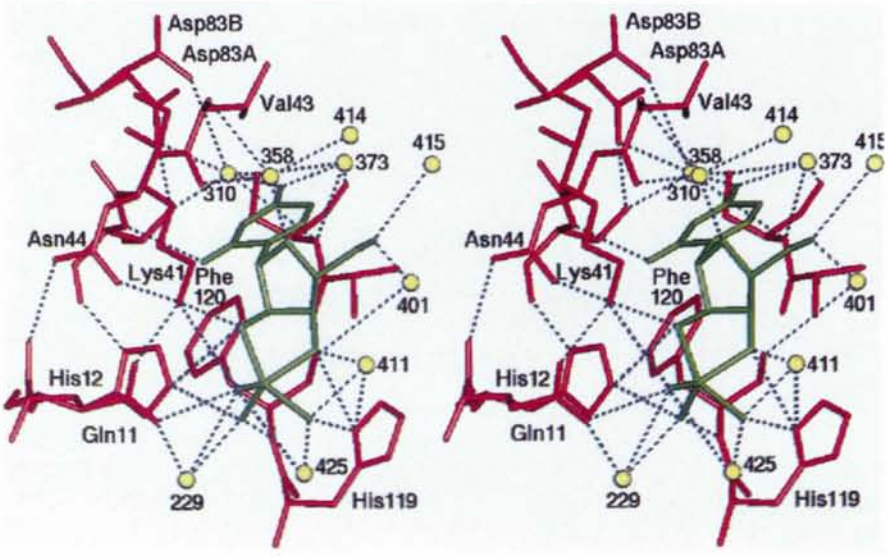

Fig. 4. The active-site region of 1RUV. Hydrogen bonds between selected atoms of the UV, the solvent and the protein are indicated with dashed lines.

Table 2. *Interatomic distances (Å) between the TBP vanadate O atoms and critical features in the RNase A active-site environment*

O2′	O3′	O1V	O2V	O3V
		1RUV		
Lys41 N^{ζ} 2.7	Wat411 2.6	His12 $N^{\varepsilon 2}$ 2.7	Gln11 $N^{\varepsilon 2}$ 2.9	Wat425 2.2
His12 $N^{\varepsilon 2}$ 3.4	His119 $N^{\delta 1}$ 3.2	Wat229 2.7	Lys41 N^{ζ} 3.3	His119 $N^{\delta 1}$ 2.6
	Phe120 O 3.3	Phe120 N 2.9	Wat425 3.5	Wat411 2.5
		6RSA		
Lys41 N^{ζ} 2.8	Wat323 2.2	His12 $N^{\varepsilon 2}$ 2.7	Gln11 $N^{\varepsilon 2}$ 2.5	Wat323 2.3
His12 $N^{\varepsilon 2}$ 3.0	His119 $N^{\delta 1}$ 2.6	Phe120 N 2.9	Lys41 N^{ζ} 3.5	His119 $N^{\delta 1}$ 2.7
		Wat322 2.9		Wat325 3.1

Wat310, Wat373, and Wat401 has been described earlier (Gilliland, Dill, Pechik, Svensson & Sjölin, 1994). Two important hydrogen-bond interactions (shown in Fig. 4) are formed directly between protein atoms and the uridine base. The peptide N of Thr45 is 2.9 Å from the uridine O2, while $O^{\gamma 1}$ of Thr45 is 2.7 Å from N3 of the uridine. Two conserved water molecules, Wat310 and Wat373, mediate the interaction of the nucleotide base with the protein to accommodate a pyrimidine base in the B_1 pocket.

The R_1 subsite includes residues His12, Lys41, Val43, His119, Phe120 and water molecules, Wat358, Wat411 and Wat414 interacting with the ribose. Several components considered part of the R_1 subsite are also part of the P_1 subsite interacting with the TBP vanadate atoms. The most significant interactions in the R_1 subsite are those associated with Val43 and Wat358. The ribose ring O4′ hydrogen bonds to Val43 O (3.4 Å), and Wat358, an essential component of the subsite, is within hydrogen-bonding distance to several R_1 components including Wat414 (3.1 Å), Val43 backbone (3.0 Å to O and 3.2 Å to N), the ribose O atom O4′ (3.1 Å) as well as Wat365 (2.8 Å) found outside the R_1 subsite. Wat411 and Wat414 are weakly associated with the R_1 subsite.

The P_1 subsite of 1RUV is composed of Gln11, His12, His119, Lys41, Phe120, and water molecules, Wat229, Wat411 and Wat425, each of which is in close contact with the TBP vanadate structure (Table 2). The position of the essential residues in the P_1 subsite, His12, Lys41, and His119, relative to the UV inhibitor is illustrated in Fig. 5. One unusually short hydrogen-bond distance of 2.2 Å is found between the apical vanadate O atom O3V and Wat425.

4.2. *Structural changes in RNase A induced by UV binding*

A comparison of 1RUV with the unligated 7RSA (Wlodawer *et al.*, 1988) provides direct insight into the structural perturbations in the enzyme induced by UV binding. Despite the necessary displacement of several well defined water molecules in the active site of the unligated enzyme (Wat203, Wat240, Wat281, and Wat271 in 7RSA), the two structures are quite similar. The overall r.m.s. deviation between the C^{α} positions is

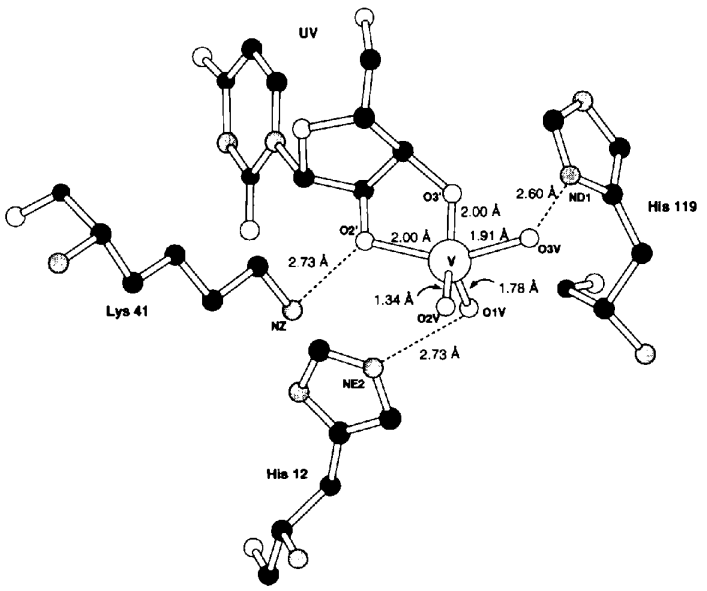

Fig. 5. The UV in the active site of 1RUV with the associated basic residues, His12, Lys41, and His119. The geometry including bond angles and distances of the TBP is shown.

0.18 Å, indicating no major conformational change upon UV binding. Lys41, Pro42, and Val43 exhibit the largest shifts in the main-chain atom position (0.4, 0.3, and 0.4 Å, respectively). The side chain of Lys41 bridges the P_1- and R_1-binding subsites, interacting directly with O2′ and O2V atoms of the bound vanadate. The difference between Lys41 N^{ζ} in the two structures is 0.9 Å. Val43 forms part of B_1 subsite making van der Waals contacts with the pyrimidine ring of the inhibitor. In 1RUV the Val43 $C^{\gamma 1}$ lies above the plane of the uridine ring at distances ranging from 3.8 to 4.2 Å to each ring atom. The only other large change that occurs upon UV binding to RNase A is the movement of the Arg85 C^{α} by 0.4 Å. Arg85 is adjacent to Val43, and, therefore, the movement is likely a consequence of the repositioning of Val43 (Svensson, Sjölin, Gilliland, Finzel & Wlodawer, 1986). Interestingly, both Arg85 and Val43 have two conformations in 7RSA, but only one in UV–RNase A. The observed conformations of the two residues in 1RUV are close to the *A* conformations in 7RSA that have occupancies of 40 and 50%, respectively.

The comparison between 1RUV and 7RSA also reveals that residues near the active site exhibit reduced *B* factors, becoming less mobile upon UV binding (Fig. 6). The most significant differences in the *B* factors occur for three residues that interact directly with the UV, Gln11, Lys41 and His119. The *B* factors are reduced by 5–15 $Å^2$. One of these residues, Gln11, adopts a single conformation in 1RUV that is different from either of the two conformations observed in 7RSA. This change may be a consequence of the strong interaction between $N^{\varepsilon 2}$ of Gln11 and O2V on the UV. As suggested earlier (Svensson *et al.*, 1986; Wlodawer *et al.*, 1988), the presence of two conformations in 7RSA results from the absence of a ligand or substrate in the active site. Lys41 and His119 also interact directly with vanadate O atoms in 1RUV, and, therefore, the reduced *B* factors for these residues are expected. The changes for Lys41 are consistent with an early report of a reduction in *B* factors for a UV–RNase A complex (Alber *et al.*, 1983). (No numerical data or coordinates are available to quantitatively assess the similarity with the results reported here.) Unexpectedly, significant changes in the *B* factors for several residues, Ser18, Gln101, Lys91, Lys98 and Lys104, far removed from the active-site region were observed. Surprisingly, the three surface lysines become more mobile as UV binds to the active site.

Like the unligated 7RSA structure, 1RUV contains a number of residues with multiple conformations. However, only four of the 11 multi-conformation residues in the UV–RNase A complex correspond to those in the 7RSA structure. Two of these four common residues in 1RUV, Ser32 and Ser50, exhibit the same conformational occupancies and *B* factors observed in 7RSA. For the other two residues, Ser77 exhibits only one common conformation, and Asp83 has no common conformations. For both Ser77 and Asp83 the *B* factors are similar, but the occupancies for Ser77 are different, 1:1 and 2:1 for 1RUV and 7RSA, respectively. Five of the remaining seven 1RUV multi-conformation residues, Ser15, Ser18, Gln28, Ser59 and Val63, are surface residues. The primary conformations found in 1RUV are similar to the single conformation found in 7RSA. In cases where the conformation occupancies are 1:1, one of the conformers agrees with that found in 7RSA. For Ser16, the conformation with lower occupancy agrees with that found in 7RSA, and for Asp24 neither conformer was observed in 7RSA.

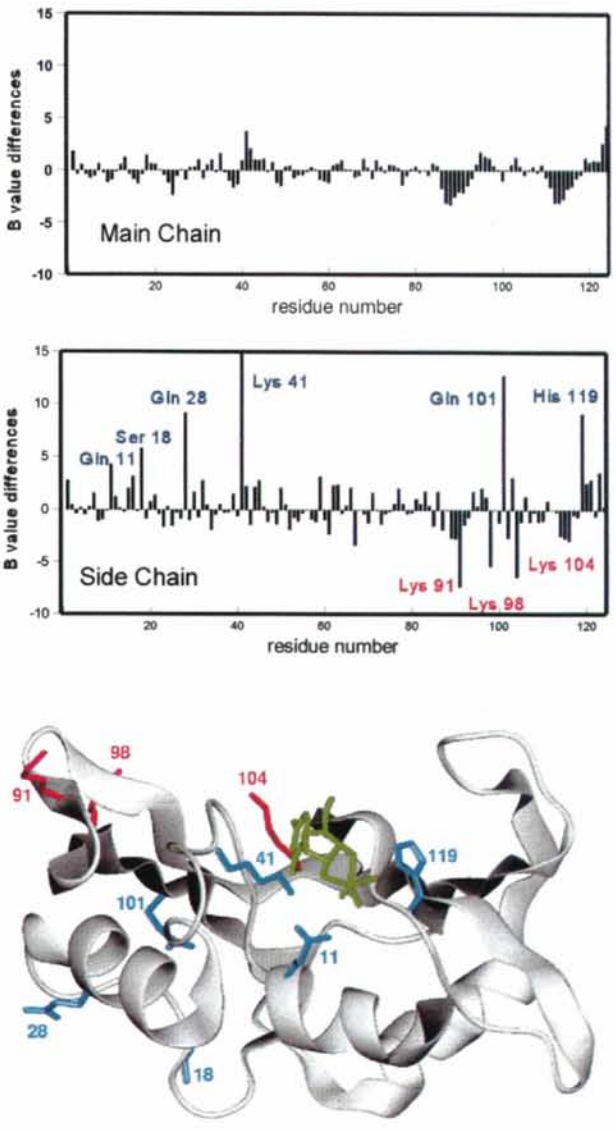

Fig. 6. Average *B*-factor differences ($Å^2$) of 7RSA–1RUV: the top graph is the average main-chain *B*-factor differences for each residue, and the bottom graph is the average side-chain *B*-factor differences for each residue. The largest differences are labeled with the residue name and number and the positions of these residues are shown in the drawing at the bottom.

Table 3. *V—O distances (Å) obtained for the intermediate and final structures of the mono- and dianionic vanadate of 1RUV and for 6RSA*

Refinement stage	V—O2′	V—O3′	V—O1V	V—O2V	V—O3V
Dianion starting model	2.00	2.07	1.60	1.60	1.93
After 30 cycles	1.98	2.04	1.71	1.53	1.94
After iterative model changes	1.99	2.01	1.80	1.42	1.94
After relaxing restraints	1.99	1.97	1.81	1.41	1.95
Monoanion starting model	1.86	1.92	1.84	1.54	1.86
After 30 cycles	1.91	1.95	1.80	1.48	1.90
After iterative model changes	1.98	1.97	1.78	1.39	1.93
After relaxing restraints	1.99	1.96	1.82	1.39	1.93
Final model	2.00	2.00	1.78	1.34	1.91
6RSA	1.88	1.90	1.91	1.75	1.75

The nine residues modeled with multiple conformations in 7RSA, but with one conformation in 1RUV, are the surface residues Gln11, Asn34, Val43, Lys61, Asn67, Arg85, Lys91, Lys98 and Lys104. Not surprisingly, many of these residues were much more mobile, as suggested by increased *B* factors, in the 7RSA compared with the 1RUV. As stated above, both Gln11 and Val43 interact directly with the UV in the active site, and Arg85 interacts with Val43 through van der Waals interactions, becoming conformationally constrained as UV binds. It was reported earlier (Svensson *et al.*, 1986) that Asp83, Arg85, and Val43, each modeled with two conformations in 7RSA, may move in concert given that Arg85 $N^{\eta 2}$ makes a hydrogen bond (3.1 Å) to Asp83*B* $O^{\delta 2}$.* The three lysines, Lys91, Lys98, and Lys104, exhibit increased *B* factors indicating high mobility making it impossible to model additional discrete conformations of the side chains. The conformations of amino acid residues Asn34, Lys61 and Asn67 in 1RUV are all similar to the conformation with the highest found in 7RSA. The *B* factors of these three residues in 1RUV are slightly elevated from those found in 7RSA. The N^{ζ} of Lys61 forms a 2.8 Å hydrogen bond with Wat298. Finally, Asn67 is involved in intermolecular contacts with a neighboring molecule in the unit cell.

4.3. *Comparison of 1RUV with the joint X-ray/neutron refined UV–RNase A (6RSA)*

Comparison of 1RUV with 6RSA, a UV–RNase A complex previously determined using a joint X-ray/neutron data (Wlodawer *et al.*, 1983) provides insight into the quality of the present structure and suggests how the refinement procedure itself may affect the outcome of the final structure. Virtually identical protocols were followed in preparing the 1RUV crystals used to collect the diffraction, and although different programs were used in the refinement process, both methods were based on the *PROLSQ* algorithm (Hendrickson & Konnert, 1980). From these similarities one would expect 1RUV to be very similar to the 6RSA. However, the two structures have a number of significant differences, particularly in the active-site region and in the UV itself. Moreover, many of these differences cannot be accounted for by uncertainties in the refinement, and therefore must result from the differences in the experimental and/or computational structure determination procedure. The obvious differences in the structure determinations that could give rise to the observed discrepancies include the enzyme sample used to produce crystals, type and resolution of diffraction data collected, data-processing software, and the UV standard groups used in the refinement in each case. In the present analysis, only X-ray data, collected to 1.3 Å resolution, was used and the UV standard groups were generated directly from the structure of model oxyvanadate compounds determined from high-level *ab initio* quantum calculations. In the 6RSA structure determination, both 2.0 Å X-ray and 2.2 Å neutron data were used, and the UV standard groups were only approximated.

As stated above, most of the differences between the two UV–RNase A structures are limited to the immediate active-site region including the UV itself, especially the TBP vanadate atoms, and amino-acid residues and bound water molecules nearby. The overall r.m.s. deviation in the backbone C^{α} positions is only 0.2 Å, with Lys1 exhibiting the largest C^{α} shift, nearly 0.5 Å. The organic portion of UV, including the uridine base and ribose ring in both structures also agrees reasonably well. The pucker of the ribose ring was determined to be 3′-*endo* in the current analysis, consistent with the classification reported in the 6RSA structure. The final ribose torsion angles in 1RUV as defined by Saenger (1983), are 2, −21, 32, −32 and 17° for ν_0 to ν_4, respectively.

Although the same general hydrogen-bonding patterns are observed in both the immediate active sites of both 1RUV and 6RSA, a number of discrepancies in the interatomic distances are observed. The UV V—O distances at various stages of the current refinement process along with those from the final 6RSA structure are summarized in Table 3 for comparison. As seen in the table, when 1RUV and 6RSA are compared, all five V—O distances differ by 0.1 Å or more, with the largest discrepancy of 0.4 Å occurring for V—O2V distance. More important, the overall bond-length patterns around the TBP vanadate in both structures are inconsistent.

* *A* and *B* refer to the primary (highest occupancy) or secondary conformers of residues modeled with two conformations.

Differences in the UV absolute structure naturally lead to differences in the final distances between the vanadate O atoms and key residues in the P_1 subsite. Summarized in Table 2 are the important interatomic distances between the vanadate O atoms in the UV and key residues of the P_1 subsite for both 1RUV and 6RSA. Considering the data in Table 3, the largest differences in the interatomic distances between the final structures are the O2′ to His12 $N^{\varepsilon 2}$, O3′ to His119 $N^{\delta 1}$, and O2V to Gln11 $N^{\varepsilon 2}$ distances, with discrepancies ranging from 0.4 to 0.5 Å. Despite the differences in relative positions, the absolute positions of the important active-site residues agree reasonablely well. The conformation of His12, Lys41 and His119 were similar with maximum differences in atomic positions of less than 1.0 Å in all cases. The Asp121 $O^{\delta 1}$ to His119 $N^{\varepsilon 2}$ distances are 2.7 and 2.9 Å, while the Thr45 O to His12 $N^{\delta 1}$ distances are 2.7 and 2.5 Å in the current and 6RSA structures, respectively. These distances are consistent with the fact that both His12 and His119 were treated as fully protonated in both refinements, indicating strong interactions occur with Thr45 and Asp121, respectively.

Besides the discrepancies in the protein–UV interaction distances between the two structures, important differences in the solvent structure are also observed. Interestingly, many of the differences in solvent structure occur for waters involved in binding of the UV in the active site. Both structures were found to contain three closely interacting water molecules in the immediate active site (Wat229, Wat411 and Wat425 in 1RUV, and Wat322, Wat323 and Wat325 in 6RSA). Of these identified waters, only Wat229 and Wat322 occupy the same relative position in the active site. The remaining waters occupy unique positions in their respective active sites.

4.4. *Trigonal bipyramid oxyvanadate structure*

Illustrated in Fig. 3 are the basic structural features of the oxyvanadate portion of the UV obtained from the final crystallographic refinement, along with primary interactions involving key residues in the enzyme active site. As seen in the figure, the penta-coordinate vanadate structure is a distorted TBP with the O2′ and O3V atoms occupying the apical positions and the O1V, O2V and O3′ atoms occupying approximate equatorial positions around the vanadium. Several angles, including O3V—V—O2′ and O3V—V—O3′ deviate significantly from those expected for a true TBP (with deviations of 29.5 and 18°, respectively). However, the most important diagnostic structural features of the vanadate are the V—O distances themselves. As seen in Fig. 5, the crystallographically determined V—O distances vary considerably, and are only qualitatively consistent with typical TBP's in which the axial bond distances are elongated relative to those in the equatorial plane (*e.g.* Crans, Felty & Miller, 1991). It is interesting to note that although the two axial V—O distances are similar (1.91 and 2.00 Å), the equatorial V—O distances are extremely asymmetric ranging from 1.34 Å for V—O2V to 2.0 Å for V—O3′.

The final structure for the oxyvanadate portion of the UV obtained from the current analysis can be compared directly with that determined previously in the 6RSA structure. As seen from the data in Table 2, a number of significant differences in the V—O distances between the two structures are evident. Most noticeably, the V—O2V and V—O3V distance were 0.4 Å shorter and 0.2 Å longer in the present structure compared with 6RSA. More important, the overall V—O bond-distance patterns are quite different. Given the similarity in the experimental conditions used in each case noted above, the discrepancies in these fundamental distances are most likely a result of differences in the resolution of the data and in the UV constraints used in the refinement for the 6RSA and 1RUV structures and the completeness of the refinement.

Comparison of the basic structural features (V—O bond distances and O—V—O angles) of the TBP oxyvanadate portion of the UV from the final X-ray refinement shown in Fig. 5 with the same features from the model oxyvanadates determined computationally (EOV^- and EOV^{2-}) shown in Figs. 1(*a*) and 1(*b*), indicates the final X-ray structure is most similar to the calculated monoanionic structure, EOV^-. Although the absolute magnitude of all the V—O bond distances around the TBP vanadium are not in complete agreement, the V—O bond-distance pattern is similar. In particular, the bond distances associated with the non-bridging equatorial O atoms (V—O1V and V—O2V) were highly asymmetric in the final X-ray refined structure, consistent with that found for the EOV^- and not EOV^{2-}. Given the dramatic effect of protonation of the electronic character of the oxyvanadates and its influence on the final structure, these data suggest that in the bound UV–RNase complex the O1V atom is protonated and the O2V atom is not, resulting in an overall monoanionic UV inhibitor.

4.5. *Solvent structure*

A total of 131 water molecules associated with the protein atoms of 1RUV have been identified in the final electron-density map. Of the total, 56 form multiple hydrogen bonds with the protein, 53 form only one hydrogen bond with the protein, and 22 are not within hydrogen-bond distance to any part of the protein, and account for the waters identified in the outer solvation shells. Most of the waters molecules form a shell covering the protein, with 82% of the total identified waters within hydrogen-bonding distance to one or more other water molecules (46 waters are within hydrogen-bonding distances to one other water molecule and 61 waters are within hydrogen-bonding distance to more than one water). Consistent with its use as a precipitant during the crystallization procedure, a single 2-methyl-2-propanol molecule was also identified in the electron-density

map and included in the refinement. The location and *B* factors of the 2-methyl-2-propanol atoms in 1RUV are similar to those observed in the unligated 7RSA structure.

As seen in Fig. 4, six water molecules, Wat229, Wat310, Wat358, Wat373, Wat411 and Wat425, are found directly interacting with the UV. Three of these active-site waters, Wat310, Wat358, Wat373, mediate the interaction of the base with the protein in the B_1 subsite, while the remaining three waters interact with the vanadate O atoms. Three additional waters, Wat401, Wat414 and Wat415 interact primarily with the O5′ ribose O atom and are far removed from the rest of the UV. Wat414 is within hydrogen-bonding distance (3.1 Å) to Wat358 in the B_1 subsite forming a hydrogen-bond network between the B_1 and R_1 subsites. As shown in Table 2, the interatomic distances between the active-site water O atoms and the important UV and protein residue heteroatoms are consistent with that expected for a standard hydrogen bond (2.5 to 3.0 Å), except for Wat425. One of the water molecules, Wat425, and the TBP axial O atom O3V is only 2.2 Å, considerably less than the interaction distances associated with other waters in the active site. Remarkably, a water molecule identified in the 6RSA structure (Wat323) is also found unusually close to O3V (2.3 Å).

5. Discussion

5.1. *Refinement process*

The results obtained from the refinement for the UV moiety in the present structure, 1RUV, and the discrepancy with that reported previously in 6RSA is disturbing and issue a warning concerning the influence of refinement techniques on the final structure. Two separate crystallographic refinements were performed using the mono- and dianion vanadate models determined computationally as the starting points for the UV. As seen in Table 3, after 30 cycles of refinement with distance restraints, the two versions of UV retained significant differences in the V—O distances. Assuming that the constraints of the UV standard group were preventing convergence, the UV standard group was replaced with the UV resulting from the refinement, and the refinement was allowed to continue. After three substitutions of the UV standard group, each followed by six cycles of refinement, the two models converged to identical structures within reasonable error limits. A second approach to eliminating the bias of the initial model was to relax all the distance restraints on the V—O distances from the beginning. The distance restraints were kept in place for the protein, and the initial starting mono- and dianionic UV models were again treated separately. After six cycles of refinement, the monoanionic and dianionic UV starting models converged to structures with the same V—O distances and these distances were also the same as those that resulted from the previously described procedure (see Table 3). Thus, a consistent model was obtained from four independent procedures.

Even though the different UV starting models from the refinement converged to a consistent final structure, the final structure differs significantly from either the mono- and dianionic starting models and from the UV of 6RSA. Since the TBP geometry of the vanadate is distorted from either of the starting models, it raises the question as to whether the vanadate structure is physically relevant. The consistency of the models does suggest that the models are relevant, but a number of possibilities exist for why this might not be the case. For example, the high resolution of the data may require anisotropic modeling of the vanadium, errors in the data or the refinement software may influence the final geometry, the vanadate may be a composite of several different structures resulting from different protonation or oxidation states of vanadium, *etc.* Nevertheless, the results obtained in the studies reported here illustrate the importance of the standard group in the outcome of the refinement.

5.2. *UV binding*

The UV is bound in the P_1, B_1, R_1 sites originally described by Richards & Wyckoff (1973). Some distances between UV and protein atoms (not including H atoms) are shown in Fig. 5. The RNase structure exhibits only subtle changes upon binding of inhibitors, however, a stabilization of the structure around the active site is suggested by the *B*-factor comparison and by the decrease in the number of residues displaying multiple conformations.

The B_1 site plays an important role in substrate binding and specificity and is presumably important for correctly orienting the substrate in relation to the catalytic groups. This site is a hydrophobic sleeve formed by a Val43 methyl group on one side and Phe120 on the other with hydrogen bonding on the interior edge to the Thr45 O^{γ} atom. The non-productive 'retro-binding' described for guanine dinucleotide inhibitors by Aguilar, Thomas, Mills, Moss & Palmer (1992) can be interpreted as a demonstration of the specificity of the site. Although guanine can fit into the site, in doing so the chain direction is opposite to that needed to place the ribose phosphate bonds in the active site. The two structures that define retro-binding, 1RNC and 1RND, still include one of the conserved waters of the active site. Both structures have a water approximately 0.7 Å away from Wat310 of 7RSA

The plot of the average *B*-factor differences, Fig. 6, shows a reduction of the *B* factors for the active-site residues Gln11, Lys41 and His119. In addition, virtually no change in the *B* factors for other residues of the active-site region is observed, particularly His12, Val43, Asn44, Thr45 and Phe120. These residues line the active-site cleft while Gln11, Lys41 and His119 form the exposed side of the active site.

5.3. *Is the trigonal bipyramid oxyvanadate structure a transition-state analog?*

Previous crystallographic structure analyses of the UV–RNase A complex focused primarily on details of the protein and the interaction of the active-site residues with the UV inhibitor. Little attention was paid to the structural features of the UV itself. Quantifying the basic structural features of the bound UV inhibitor in the 1RUV is, however, an essential first step in answering questions regarding the applicability of oxyvanadates as true phosphorane analogs and the implication of the UV structure on the actual RNase A enzymatic mechanism.

The significant distortions of the TBP noted above suggest that the bonding interaction involving the O atoms surrounding the vanadium are atypical and are influenced by factors other than those expected for a typical TBP transition metal complex. The latter may be more appropriate given the influence of the active-site environment on the vanadate structure, clearly evident from the data in Fig. 5 and in Table 2. Each of the vanadate O atoms interacts primarily with only one protein component in the RNase A active site. O1V interacts with $N^{\varepsilon 2}$ of His12, O2V interacts with $N^{\varepsilon 2}$ of Gln11, O3V interacts with $N^{\delta 1}$ of His119, O2′ interacts with N^{ζ} of Lys41, and O3′ interacts primarily with $N^{\delta 1}$ of His119. Distortion of the TBP oxyvanadate framework is consistent with these important interactions, disrupting the TBP arrangement to optimize interactions with the active site. This is most noticeable for O3V displaced out of the apical plane and towards $N^{\delta 1}$ of His119, in order to achieve the short 2.6 Å interatomic distance. Without these distortions the five vanadate O atoms probably could not form close contacts with the protein atoms. Apparently, the electronic structure of the TBP oxyvanadate is such that significant distortions of the TBP framework are possible to allow for necessary interactions with the active site, and may provide the explanation for the ability of UV to act as a strong inhibitor despite electronic differences with the corresponding phosphorane reported previously.

5.4. *Protonation of the UV*

One of the most relevant questions concerning the structure of 1RUV is the protonation state of the UV in the RNase A active site. The protonation state at various stages along the reaction pathway of the actual RNase A enzymatic mechanism, including the proposed TBP phosphorane structure, has been an issue of considerable debate for many years. Some have argued that stabilization of key intermediates or transition states is made possible primarily through proton transfer to the developing anionic phosphorane. To the extent that the electrostatics of the UV mimics those of the true TBP phosphorane, the protonation state of the UV should provide insight into the nature of the corresponding phosphorane. Determining the proton positions directly from X-ray crystallographic data is, however, a non-trivial task. Although protons cannot be observed directly in the electron-density map obtained from the X-ray diffraction data, their presence (or absence) can be inferred, in certain cases, from the relative positions of the heavy atoms. If the electronic and geometric structure of the system is strongly influenced by the overall protonation state, geometric patterns can be used to predict the most probable protonation state of the system. The structure of 1RUV offers a detailed description of the penta-coordinated vanadium. As shown in Fig. 5, the distribution of the V—O distances surrounding the vanadium in the complex agrees more closely with the distribution found in the monoanion oxyvanadate model compound as compared to the dianionic model. The distribution in the 6RSA structure, on the other hand, points neither toward the monoanion nor the dianion. This appears to be the case for the UV in the 1RUV structure.

Although the comparative data is reasonably suggestive that the UV in the RNase A active site is monoanionic, there are a number of unexplained structural differences in the final X-ray refined UV–RNase structure and the monoanionic computational model, EVO^-. The most noticeable of these differences is the V—O distances themselves that differ by as much as 0.2 Å. Specifically, the equatorial V—O2V distance is exceedingly short in the final X-ray refined structure (1.34 Å), over 0.2 Å shorter than the shortest V—O distance in EOV^-. The remaining V—O distances were all longer in the X-ray structure compared with those determined computationally for EOV^- by 0.1 Å or less. A number of differences in the O—V—O angles ranging from as little as 3° to as much as 27° for O2V—V—O3′ are also observed.

Most of these discrepancies in the experimental and theoretical UV structural features mentioned above can be accounted for from uncertainties in the respective data. Absolute errors as high as 0.1 Å in the bond distances and 10° in the bond angels are expected. Discrepancies in the V—O2V distance (0.2–0.4 Å depend on the level of theory), however, are unlikely to be the result of systematic error. Moreover, the exceedingly short UV V—O2V bond distance found crystallographically is also inconsistent with the V—O distances obtained from the crystal structures of small model penta-coordinate oxyvanadate compounds (*e.g.* Crans *et al.*, 1991; Angus-Dunne, Batchelor, Tracey & Einstein, 1995). At least two possible reasons for the distortion may be given. First, experimental or computational factors may have influenced the refinement and hence the interpretation of the vanadate structure. This seems unlikely because of the care taken to insure convergence of the crystallographic refinement. A second perhaps more probable reason is that the protein electrostatic environment is introducing significant perturbations in the electronic structure of the vanadate. One might con-

ceptualize this as the enzyme influencing the structure of the vanadate to adopt a phosphorane-like transition state.

Assuming that the above mentioned experimental discrepancies are not dominating and that the observe electron density accounts for a single UV moiety, the highly asymmetric non-bridging vanadyl V—O distances cannot be accounted for without an asymmetric monoanion protonation of this group. Further experimental and computational work to probe this latter hypothesis is currently under way.

The authors would like to thank Morris Krauss and Walter Stevens for helpful discussions

References

Aguilar, C. F., Thomas, P. J., Mills, A., Moss, D. S. & Palmer, R. A. (1992). *J. Mol. Biol.* **224**, 265–267.

Alber, T., Gilbert, W. A., Ponzi, D. R. & Petsko, G. A. (1983). *Ciba Found. Symp.* **93**, 4–24.

Angus-Dunne, S. J., Batchelor, R. J., Tracey, A. S. & Einstein, F. W. B. (1995). *J. Am. Chem. Soc.* **117**, 5292–5296.

Avey, H. P., Boles, M. O., Carlisle, C. H., Evans, S. A., Morris, S. J., Palmer, R. A., Woolhouse, B. A. & Shall, S. (1967). *Nature (London)*, **213**, 557–562.

Bernstein, F. C., Koetzle, T. F., Williams, G. J. B., Meyer, E. F. Jr, Brice, M. D., Rogers, J. R., Kennard, O., Shimanouchi, T. & Tasumi, M. (1977). *J. Mol. Biol.* **112**, 535–542.

Borah, B., Chen, C., Egan, W., Miller, M., Wlodawer, A. & Cohen, J. S. (1985). *Biochemistry*, **24**, 2058–2067.

Borkakoti, N., Moss, D. S., Stanford, M. J. & Palmer, R. (1984). *J. Crystallogr. Spectrosc. Res.* **14**, 467–494.

Campbell, R. & Petsko, G. A. (1987). *Biochemistry*, **26**, 8579–8584.

Crans, D. C., Felty, R. A. & Miller, M. M. (1991). *J. Am. Chem. Soc.* **113**, 265–269.

Crans, D. C., Willging, E. M. & Butler, S. R. (1990). *J. Am. Chem. Soc.* **112**, 427–432.

Finzel, B. C. (1987). *J. Appl. Cryst.* **20**, 53–55.

Frisch, M. J., Trucks, G. W., Head-Gordon, M., Gill, P. M. W., Wong, M. W., Foresman, J. B., Johnson, B. G., Schlegel, H. B., Robb, M. A., Replogle, E. S., Gomperts, R., Andres, J. L., Raghavachari, K., Binkley, J. S., Gonzalez, C., Martin, R. L., Fox, D. J., Defrees, D. J., Baker, J., Stewart, J. J. P. & Pople, J. A. (1992). *GAUSSIAN92, Revision A*, Gaussian, Inc., Pittsburgh, PA, USA.

Gilliland, G. L., Dill, J., Pechik, I., Svensson, L. A. & Sjölin, L. (1994). *Protein Pept. Lett.* **1**, 60–65.

Hehre, W. J., Radom, L., Schleyer, P. v. R. & Pople, J. A. (1986). *Ab Initio Molecular Orbital Theory*. New York: Wiley-Interscience.

Hendrickson, W. & Konnert, J. (1980). *Computing in Crystallography*, edited by R. Diamond, S. Ramaseshan & K. Venkatesan, pp. 1301–1323. Bangalore: Indian Academy of Sciences.

Howard, A. J., Gilliland, G. L., Finzel, B. C., Poulos, T. L., Ohlendorf, D. H. & Salemme, F. R. (1987). *J. Appl. Cryst.* **20**, 383–387.

Howlin, B., Harris, G. W., Moss, D. S. & Palmer, R. A. (1987). *J. Mol. Biol.* **196**, 159–164.

Jones, T. A. (1978). *J. Appl. Cryst.* **11**, 268–272.

Jones, T. A., Zou, J.-Y., Cowan, S. W. & Kjeldgaard, M. (1991). *Acta Cryst.* A**47**, 110–119.

Kartha, G., Bello, J. & Harker, D. (1967). *Nature (London)*, **213**, 862–865.

Kim, E. E., Varadarajan, R., Wyckoff, H. W. & Richards, F. M. (1992). *Biochemistry*, **31**, 12304–12314.

Kostrewa, D., Choe, W.-W., Heinemann, U. & Saenger, W. (1989). *Biochemistry*, **28**, 7592–7600.

Krauss, M. & Basch, H. (1992). *J. Am. Chem. Soc.* **114**, 3630–3634.

Lindquist, R. N., Lynn, J. L. & Lienhard, G. E. (1973). *J. Am. Chem. Soc.* **95**, 8762–8768.

Lindqvist, Y., Schneider, G. & Vihko, P. (1994). *Eur. J. Biochem.* **221**, 139–142.

Martin, P. D., Doscher, M. S. & Edwards, B. F. P. (1987). *J. Biol. Chem.* **262**, 15930–15938.

Richards, F. M. & Vithayathil, P. J. (1959). *J. Biol. Chem.* **234**, 1459–1465.

Richards, F. M. & Wyckoff, H. W. (1971). *The Enzymes*, Vol. 4, 3rd ed., edited by P. D. Boyer, pp. 647–806. New York: Academic Press.

Richards, F. M. & Wyckoff, H. W. (1973). *Atlas of Molecular Structures in Biology*, Vol. 1, edited by D. C. Phillips & F. M. Richards, pp. 1–75. Oxford: Clarendon Press.

Satow, Y., Cohen, G. H., Padlan, E. A. & Davies, D. R. (1986). *J. Mol. Biol.* **190**, 593–604.

Saenger, W. (1983). *Principles of Nucleic Acid Structure*, pp. 17–21. New York: Springer-Verlag.

Sheriff, S. (1987). *J. Appl. Cryst.* **20**, 55–57.

Svensson, L. A., Sjölin, L., Dill, J. & Gilliland, G. L. (1991). *Structure, Mechanism and Function of Ribonucleases*, edited by C. M. Cuchillo, R. de Llorens, M. V. Nogues & X. Pares, pp. 31–38. Spain: Universitat Autonoma de Barcelona/IBF Publications.

Svensson, L. A., Sjölin, L., Gilliland, G. L., Finzel, B. C. & Wlodawer, A. (1986). *Proteins Struct. Funct. Genet.* **1**, 370–375.

Taylor, H. C., Kormoriya, A. & Chaiken, I. M. (1985). *Proc. Natl Acad. Sci. USA*, **82**, 6423–6426.

Usher, D. A., Erenrich, E. S. & Eckstein, F. (1972). *Proc. Natl Acad. Sci. USA*, **69**, 115–118.

Usher, D. A., Richardson, D. I. & Eckstein, F. (1970). *Nature (London)*, **228**, 663–665.

Varadarajan, R. & Richards, F. M. (1992). *Biochemistry*, **31**, 12315–12327.

Veenstra, T. D. & Lee, L. (1994). *Biophys. J.* **67**, 331–335.

Wachters, A. J. H. (1970). *J. Chem. Phys.* **52**, 1033–1036.

Wlodawer, A., Bott, R. & Sjölin, L. (1982). *J. Biol. Chem.* **257**, 1325–1332.

Wlodawer, A., Miller, M. & Sjölin, L. (1983). *Proc. Natl Acad. Sci. USA*, **80**, 3628–3631.

Wlodawer, A. & Sjölin, L. (1983). *Biochemistry*, **22**, 2720–2728.

Wlodawer, A., Svensson, L. A., Sjölin, L. & Gilliland, G. L. (1988). *Biochemistry*, **27**, 2705–2717.

Wodak, S. Y., Liu, M. Y. & Wyckoff, H. W. (1977). *J. Mol. Biol.* **116**, 855–875.

Wyckoff, H. W., Tsernoglou, D., Hanson, A. W., Knox, J. R., Lee, B. & Richards, F. M. (1970). *J. Biol. Chem.* **245**, 305–328.

Zegers, I., Maes, D., Dao-Thi, M.-H., Poortmans, F., Palmer, R. & Wyns, L. (1994). *Protein Sci.* **3**, 2322–2339.